



Science Arts & Métiers (SAM)

is an open access repository that collects the work of Arts et Métiers Institute of Technology researchers and makes it freely available over the web where possible.

This is an author-deposited version published in: <https://sam.ensam.eu>
Handle ID: <http://hdl.handle.net/10985/17249>

To cite this version :

Franck GIROT, Frédéric DAU, Esther GUTIERREZ-ORRANTIA - New analytical model for delamination of CFRP during drilling - Journal of Materials Processing Technology - Vol. 240, p.332-343 - 2017

Any correspondence concerning this service should be sent to the repository

Administrator : scienceouverte@ensam.eu



New analytical model for delamination of CFRP during drilling

Franck Girot (Pr.)^{a,d,*}, Frédéric Dau^c, M^a Esther Gutiérrez-Orrantia^b

^a University of the Basque Country, UPV/EHU, Faculty of Engineering, Department of Mechanical Engineering, Alameda de Urquijo s/n, 48013 Bilbao, Bizkaia, Spain

^b University of the Basque Country, UPV/EHU, Faculty of Engineering, Department of Applied Mathematics, Alameda de Urquijo s/n, 48013 Bilbao, Bizkaia, Spain

^c I2M, Université de Bordeaux, Arts et Métiers ParisTech, Talence, France

^d IKERBASQUE, Basque Foundation for Science, Bilbao, Spain

A B S T R A C T

Drilling of composite material structure is a widely used process in aeronautical assembly due to its best manufacturing value (ratio quality/cost). However, delamination which can be generated at the hole exit is still a problem and is directly related to the drill axial force, the composite material mechanical characteristics and the load distribution along the cutting and chisel edges. This paper analyzes the distribution of the load along the drill edges and points out a triangular distribution associated to an additional load located at the centre of the drill. This additional load depends strongly on the feed rate. An orthotropic analytical model is then proposed in order to determine the delamination critical thrust during drilling for different combined loadings. This new model is compared with the existing ones in the literature and with experimental results. This analysis highlights that delamination occurs in a mixed mode and not in mode I only. The use of the B-K criterion for the determination of the equivalent critical energy release rate G_c and a cutting edge combined loading (triangular distribution associated to an additional load) allow a close correlation between experimental measurements and the prediction of this new model.

Keywords:

Carbon fiber reinforced polymer
Delamination
Analytical modelling
Machining

1. Introduction

The development of large civil aircrafts (Airbus A380, Airbus A350, Boeing 787 . . .) is associated with an increased use of composite materials to reduce the weight of the plane while maintaining high specific characteristics. The widespread use of these materials in aircraft structures has become a necessity and must be achieved within certain requirements such as adequate load transfer from one structural element to another via joining. The latter, usually bolted or riveted, presents performances that depend heavily on the quality and dimensional accuracy of the drilled holes. Persson et al. (1997) pointed out the effects of drilling defects on strength and fatigue life of composite laminates. The results of the static testing showed that damaged specimens yielded significantly lower

strengths (about 11%) than effect-free specimens. At 10^6 cycles, damaged specimens yielded substantially lower strengths (19%).

Although non-conventional means have been developed in the recent years (laser drilling, water jet drilling, ultrasonic . . .), drilling using cutting tool is still the most common process to achieve the best manufacturing value (ratio quality/cost).

Industrial challenges of drilling composite materials are now relatively clear. As defined by Airbus, Bombardier or Embraer in their Aerospace Process Specifications, they consist in several requirements: (i) a dimensional accuracy of IT grade 9 (for high load transfer holes) with a roughness R_a of less than $125\text{ }\mu\text{m}$, (ii) delamination of one ply over 2.54 mm around the hole whatever its diameter, (iii) tool lifetime sufficiently long without improving the price per hole compared with aluminum or steel, (iv) in stacks made of only CFRP or hybrid materials (CFRP/metallic assemblies).

Drilling holes in composite structures is significantly different than drilling holes in metallic parts. Most of the problems encountered are associated with the drilling quality. The different types of damage induced by the drill are as follows.

Thermal damage (matrix softening or burning . . .) is due to the friction between the tool and the CFRP material and depends primarily on the margin width in contact with the borehole wall,

* Corresponding author at: University of the Basque Country, UPV/EHU, Faculty of Engineering, Department of Mechanical Engineering, Alameda de Urquijo s/n, 48013 Bilbao, Bizkaia, Spain.

E-mail addresses: frank.girot@ehu.eus, franck.girot@ensam.eu (F. Girot), frederic.dau@ensam.eu (F. Dau), esther.gutierrez@ehu.eus (M.E. Gutiérrez-Orrantia).

associated with inadequate cutting conditions (high cutting speed and low feed rate). Consequently, the matrix is removed locally and the fiber reinforcement uncovered.

Brinksmeier et al. (2011) investigated different process parameters and their influence on surface integrity of the borehole. This was accomplished by measuring the cutting temperatures and forces. The investigations revealed that the use of high cutting speeds leads to increasing borehole surface layer damage in the CFRP material.

Jawahir et al. (2011) showed that this phenomenon is easily manageable controlling the spindle rotation speed (or tool cutting speed).

Park et al. (2013) developed and used empirical equations to model and analyze thermal damage and chip removal during the drilling process.

Montoya (2013) demonstrated that the temperature field near the tool/chip interface influences significantly the tool life. This temperature field is difficult to reach by experimentation, but can be obtained using numerical simulation of the workpiece thermal solicitations. The model developed allowed, by the use of an inverse method, to determine the hole wall temperature. Temperatures between 60 and 120°C can be reached depending on the cutting conditions.

Mechanical damage (top and bottom delamination, fiber bundle tearing off the machined surface, spalling, uncut fibers, uncut resin, cracking, ...) results in the generation of defects, of which the most problematic one is delamination (at entry or exit of the drill within the material) and fiber bundle tearing off as pointed out by Ho-Cheng and Dharan (1990) or Jain and Yang (1993). This residual damage, depending on its size and occurrence, leads to lower mechanical properties for the CFRP material and in particular reduces the strength and the tensile fatigue endurance limit as shown by Brinksmeier et al. (2011) or Saleem et al. (2013).

Fiber bundle tearing off occurs on the surface of the hole for a particular orientation of the laminate ply with respect to the feed rate of the tool (-45°) associated with a loss of tool edge sharpness. It results in fiber bundles which are torn off the surface of the hole, this phenomenon being repeated for each ply in the same angular orientation between the tool and the fibers. To date no model has been developed to reflect the occurrence of this phenomenon.

Infeed side delamination (or peel-up delamination) is a damage which does not appear systematically. It is associated with the combined action of the helix angle, the drilling torque and the shape of the flute as demonstrated by Ho-Cheng and Dharan (1990) or Lachaud et al. (2001). It occurs by sliding the first plies up the flutes of the drill similar to the action of a corkscrew. This vertical action separates the first plies of the material and creates a delaminated area by fracture in Mode III loading (Fig. 1a). It can also be caused by unfavorable cutting conditions upon which the fibers are not cut sufficiently. Fiber fringes are being pulled up and cause delamination also according to mode I.

Hole exit delamination (or push-out delamination) occurs when the composite plate is not supported in its bottom part and when the drill is ready to exit the material as pointed out by Ho-Cheng and Dharan (1990) or Jain and Yang (1993, 1994). When there are few plies left to drill, the rigidity reduction of the material makes the deformation easier and in particular the bending of this area of the plate. The penetration force of the drill may then be sufficient to cause the rupture of the interlayers and to allow the generation of a delaminated area when the tool exits the part (Fig. 1b). The fracture of the bottom surface plies occurs by both mode I and mode II fracture.

This type of delamination is more problematic since it is systematically repaired and therefore has an added manufacturing cost. De Zarate-Knorr (2014) pointed out that although this type of defect represents only 6% of the total damages associated with the drilling

process, compared with 27% for oval holes, repairing the delaminated area takes 5 to 6 h per hole versus 10 to 15 min for an oval hole.

This is why it is important to control this phenomenon and to be able to predict when the drill starts to generate such default due to its wear and/or to inadequate cutting conditions. It has been pointed out by various authors that the axial or thrust force is a good indicator for controlling this damage. In addition, the optimal thrust force for no delamination can be used to control the drilling machine with thrust force feedback for maximizing productivity. The axial load can be controlled in real time and the feed rate decreased when the recorded axial load approaches the critical value.

The study presented below has therefore focused on carrying out (i) correlations between cutting forces and damage, mainly delamination at the exit of the hole, by defining different analytical models which take into account the loading on the drill cutting edge, (ii) experimental evaluation of the cutting edge loading as a function of the feed rate, and (iii) comparison of the models predictions with experimental data. The originality of this work is based on (i) an analytical approach which takes into account the coupling between bending and stretching commonly observed in CFRPs with various lay-ups, and (ii) an experimental approach which identifies the thrust force distribution along the cutting edge for different feed rate of the tool.

2. Models review for delamination prediction

Among the different existing models, the most interesting ones are presented thereafter. They can be classified according to the hypothesis made on the CFRP remaining to be drilled.

2.1. Model with isotropic hypothesis: Ho-Cheng and Dharan's model

The first model was developed by Ho-Cheng and Dharan (1990) assuming that the material is isotropic and the axial force is located at the center of the hole. The critical load is expressed as:

$$F_{CRIT} = \pi \sqrt{\frac{8 \cdot G_{IC} \cdot E \cdot h^3}{3 \cdot (1 - \nu^2)}} \quad (1)$$

Where h is the plate thickness beneath the drill, G_{IC} the energy release rate in mode I, E the equivalent Young's modulus and ν the homogenized Poisson's coefficient of the plate under consideration. This model does not take into account the effect of anisotropy in the located bending or the thrust force distribution on the cutting edge. The model seems to be more adapted to drills with point angle less than 90° .

Hocheng and Tsao (2003, 2005, 2006), Tsao and Hocheng (2003, 2004, 2007, 2008) and Tsao et al. (2012) made later various contributions to develop other models of loading such as a force applied at two points, three points, a concentric loading, ... are for instance considered.

2.2. Models with orthotropic hypothesis

2.2.1. Jain and Yang's model; Zhang's model

Jain and Yang (1993, 1994) and Zhang et al. (2001) incorporate the anisotropy of the material, and assume that the axial force is located at the center. Most of the analytical models consider the presence of a circular crack for the delamination process. This assumption is more realistic for quasi-isotropic composites materials than for unidirectional ones, where an elliptical crack can be observed. Jain and Yang, then Zhang et al. have developed such a model of critical load, which incorporates the coupling between

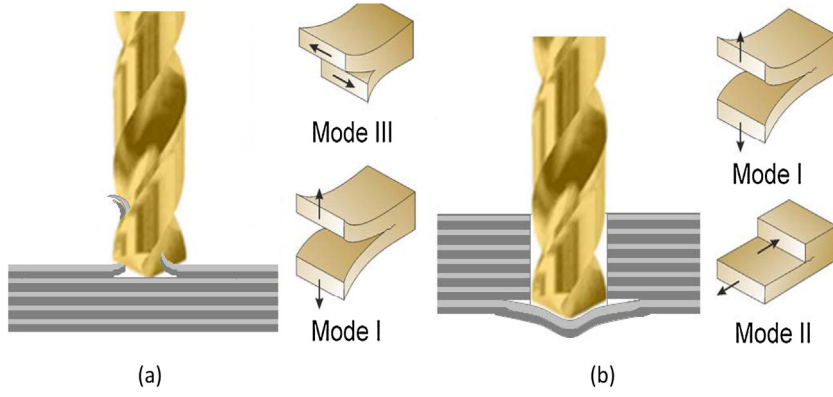


Fig. 1. Action mode of a drill leading to (a) hole entrance delamination and (b) hole exit delamination.

bending and stretching commonly observed in CFRPs with various lay-ups.

$$F_{crit} = \frac{3}{\xi} \cdot \frac{\pi}{\sqrt{2}} \cdot G_{IC} \cdot D_C^* \quad (2)$$

Where

$$D_C^* = D_{11} + \frac{2(D_{12} + 2D_{66})}{3} \xi^2 + D_{22} \xi^4 \quad (3)$$

and $\xi = a/b$ is the ellipticity ratio with a and b the half major and minor axes of the elliptical crack. Jain and Yang have minimized the critical load with respect to the ellipticity ratio since the objective is to eliminate delamination altogether. This results in a value of the ellipticity ratio of $\xi = a/b = (D_{11}/D_{22})^{1/4}$, and when this value is substituted in Eq. (2), the expression for critical thrust force for delamination becomes:

$$F_{crit} = 3 \cdot \pi \cdot \sqrt[4]{\frac{D_{11}}{D_{22}}} \cdot \sqrt{2 \cdot G_{IC} \cdot D_C^*} \quad (4)$$

with

$$D_C^* = 2 \cdot D_{11} + \frac{2(D_{12} + 2 \cdot D_{66})}{3} \sqrt{\frac{D_{11}}{D_{22}}} \quad (5)$$

where the D_{ij} coefficients refer to the bending stiffness matrix of the Classical Laminate Theory. Tsao and Chen (1997) completed this model with an analytical approach for the determination of the position of the onset of delamination during the drilling of composite laminates based on linear elastic fracture mechanics. This model does not take into account the thrust force distribution on the cutting edge.

2.2.2. Piquet's model

Piquet et al. (2000) assume that the composite is anisotropic, the applied load is equivalent to a uniformly distributed pressure q over the section of the hole, and the delamination shape is circular. The critical load is then expressed as:

$$F_{A,Crit} = 8 \cdot \pi \cdot \sqrt{\frac{G_{IC} \cdot D}{\frac{1}{3} - \frac{D'}{8 \cdot D}}} \quad (6)$$

with

$$D = \frac{1}{8} (3D_{11} + 2D_{12} + 4D_{66} + 3D_{22}) \quad (7)$$

$$D' = \frac{D_{11} + D_{22}}{2} + \frac{D_{12} + D_{66}}{3} \quad (8)$$

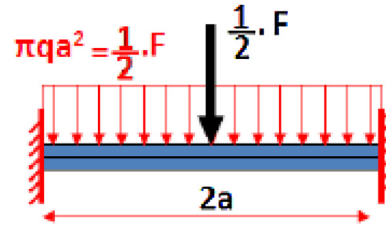


Fig. 2. Clamped plate subjected to a point loading combined to uniformly distributed loading.

2.2.3. Lachaud's model

Lachaud et al. (2001) assume that the composite is anisotropic, the load is located at the center of the hole and delamination area has a circular shape. They express the critical load as:

$$F_{crit} = 8 \cdot \pi \cdot \sqrt{\frac{2 \cdot G_{IC} \cdot D}{1 - \frac{D'}{8D}}} \quad (9)$$

It is a simple model which takes into account an orthotropic behavior of the material and is applicable for a drill point angle lower than 90° .

2.2.4. Rahmé's model

Rahmé et al. (2011) assume that the composite is anisotropic and model the effect of the drill web by a point loading and the effect of the two cutting edges by a loading uniformly distributed over the circular plate (Fig. 2). The delamination shape is supposed to be circular.

Assuming linearity, the principle of superimposition is used. The energies of deformation and of external loads are calculated from the two cases of simple loading, point loading and uniformly distributed loading. The final result is the sum of the results obtained for each case. The stress on the drill web is supposed to be equal to the stress on the cutting edges.

The critical load for delamination is assessed by Eq. (10):

$$F_{crit} = 16 \cdot \pi \cdot \sqrt{\frac{6 \cdot G_{IC} \cdot D}{13}} \quad (10)$$

This model takes into account Piquet's approach, makes a difference between the loads on the web and the lips but it does not reflect reality since the repartition of the load between the cutting edges and the drill web can be different from 0.5. Zitouné and Collombet (2007) have pointed out this aspect in a numerical simulation whose results are in good agreement with experiments. In that case, the coefficient of repartition α of the total load on the chisel edge was 0.4 for the drill they used.

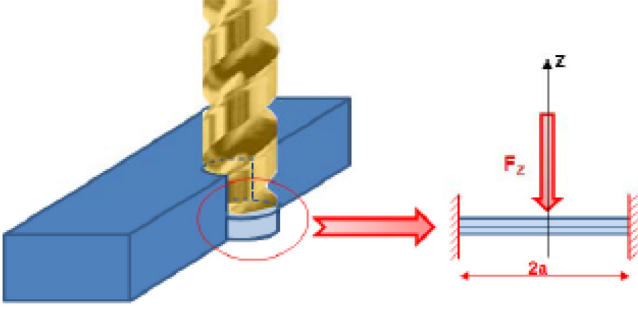


Fig. 3. Schematic representation of the model used for simulation.

2.3. FEM simulation

Zitouné and Collombet (2007) proposed a FEM analysis to calculate the thrust forces responsible for the defect at the exit of the hole during the drilling phase of CFRP structures, within a quasi-static framework. Zitouné (2013) completed this approach assuming the presence of a circular crack at the web diameter of the drill (and not at the nominal diameter as analytical models assumed) and a different distribution of the axial force on the web and of the cutting edges. Iliescu et al. (2010) proposed a simulation based on DEM to describe and optimize the process. The drawback of these solutions still lies in too long computation times (one week for simulating the drilling of a 10 mm thick plate).

2.4. Model methodology

The material to drill is supposed to behave as a cylindrical plate clamped at its ends. The drill is perpendicular to the plane formed by the structural plate and applies a bending load perpendicular to its plane (Fig. 3). When the force feeding the drill reaches a critical value F_{Zcrit} , debonding occurs between the plies.

This crack is usually initiated and propagates in a resin rich area. For isotropic materials and unidirectional plies, Hocheng and Dharan (1990) and Jain and Yang (1993) proposed an elliptical fracture surface with the major axis of the ellipse being collinear with the longitudinal direction of the fibers. But in the case of a multilayered composite plate, as a first approach, the delaminated area can reasonably be considered as circular. They assumed a mode I of delamination corresponding to debonding under the action of σ_{zz} stresses. In this paper a mixed-mode I/II and an equivalent critical energy release rate G_c will be considered.

For a multi-stack sequence, the delaminated area is modeled by an orthotropic circular thin plate embedded on its edge and transversely loaded. Its diameter corresponds to the diameter of the drill and its thickness is updated during the advance of the tool. This assumption has been verified performing drillings at different steps of the drill exit. Fig. 4 shows that for the CFRP material used, the delamination crack has its origin at the drill corner and not at the web diameter of the drill as reported by et al. (2013).

The contact action tool/plate is modeled by a resulting load F_z , depending on the particular cutting edge loading (located, uniformly distributed, triangular...). From the equilibrium equation of the plate, Timoshenko and Woinowski-Krieger (1987) determined the differential equation of the deflection w of this thin plate as:

$$2\pi r \frac{d}{dr} \left[\frac{1}{r} \frac{d}{dr} \left(r \frac{dw}{dr} \right) \right] = 2\pi r \frac{Q}{D} = \frac{F_z}{D} \text{ or } \frac{1}{r} \frac{d}{dr} \left\{ r \frac{d}{dr} \left[\frac{1}{r} \frac{d}{dr} \left(r \frac{dw}{dr} \right) \right] \right\} = \frac{q}{D} \quad (11)$$

where D is defined in Eq. (7), Q is the shearing force per unit length related to q , the uniformly distributed pressure on the circular part of the plate as:

$$Q 2\pi r = \int_0^r q 2\pi u du \quad (12)$$

The behavior of the symmetric laminated plate is defined using the Classical Laminated Theory (CLT).

To determine the deflection after integrating Eq. (11), the following boundary conditions are used:

$$w(a) = 0 \partial w(0)/\partial r = 0 \partial w(a)/\partial r = 0$$

The determination of the critical thrust force F_z uses an energy approach based on the application of the virtual work theorem to balance the delaminated plate part. The parameter that varies virtually is the radius "a" of the delaminated area:

$$\delta W_{ext} = \delta U + \delta U_d \quad (13)$$

where δW_{ext} is the virtual work of the drill load F_z ; δU the virtual variation of the strain energy of the plate and δU_d the virtual variation of the energy of delamination. The energy dissipated by the tool/chip contact is not taken into account.

The strain energy of the circular plate can be expressed as:

$$2U = U_{11} + U_{22} + U_{12} + U_{66} \quad (14)$$

Where:

$$U_{11} = \int_0^{2\pi} \int_0^a D_{11} \left(\frac{\partial^2 w}{\partial r^2} \cos^2 \theta + \frac{\partial w}{\partial r} \frac{\sin^2 \theta}{r} \right)^2 r dr d\theta \quad (15)$$

$$U_{22} = \int_0^{2\pi} \int_0^a D_{22} \left(\frac{\partial^2 w}{\partial r^2} \sin^2 \theta + \frac{\partial w}{\partial r} \frac{\cos^2 \theta}{r} \right)^2 r dr d\theta \quad (16)$$

$$U_{12} = \int_0^{2\pi} \int_0^a 2D_{12} \left(\frac{\partial^2 w}{\partial r^2} \cos^2 \theta + \frac{\partial w}{\partial r} \frac{\sin^2 \theta}{r} \right) \left(\frac{\partial^2 w}{\partial r^2} \sin^2 \theta + \frac{\partial w}{\partial r} \frac{\cos^2 \theta}{r} \right) r dr d\theta \quad (17)$$

$$U_{66} = \int_0^{2\pi} \int_0^a 2D_{66} \left(\cos \theta \sin \theta \frac{\partial^2 w}{\partial r^2} - \frac{\cos \theta \sin \theta}{r} \frac{\partial w}{\partial r} \right) r dr d\theta \quad (18)$$

The virtual work of the external forces depends on the nature of this effort (point load, uniformly distributed load, triangular load ...) and will be subsequently developed for each particular case.

The energy of delamination U_d is determined from the product of the critical energy release rate in mixed-mode (G_c) by the fracture surface assumed to be circular here. It is expressed as Eq. (19) when all the surface is delaminated:

$$U_d = G_c \pi a^2 \quad (19)$$

The equilibrium Eq. (13) can be written by using Eq. (14) to (18) and adding the expression of the virtual work of the external forces. It must be verified irrespective of the variation of the virtual radius "a", which makes it possible to determine the critical thrust force which leads to delamination. In the following, this approach is applied to different individual cases or combined loading in accordance with the conclusions of Section 3.

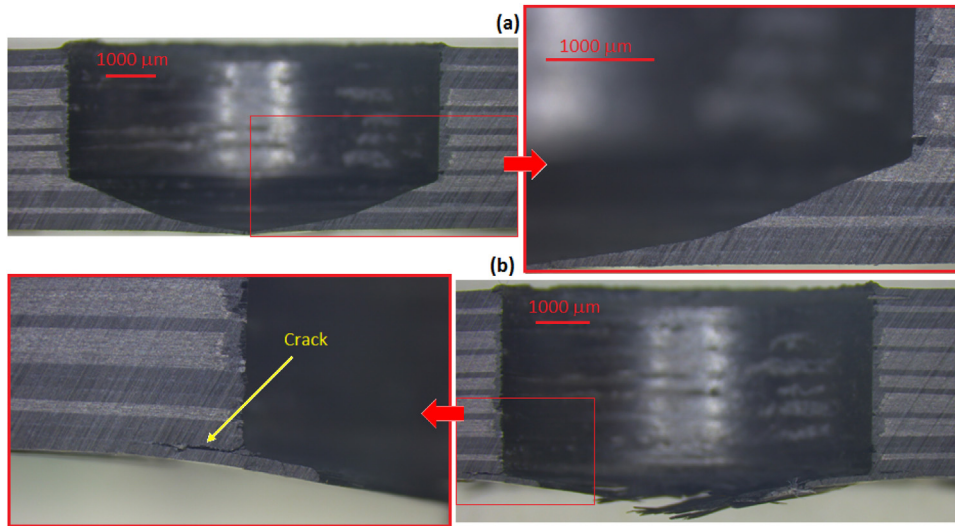


Fig. 4. Origin of crack initiation: (a) just before the exit of the drill point – no cracks are present within the material; (b) during the exit of the drill point – crack is initiated at the drill corner.

Table 1

Values of the critical energy release rates G_{IC} and G_{IIc} for different CFRP materials, at different temperatures and shear strain rate.

Authors	Material	Disorientation between plies	Temperature	Static or Dynamic	G_{IC} J/m ²	G_{IIc} J/m ²
Kusaka et al. (1994)	Besflight IM-600/Epoxy	0°	20 °C	S (10^{-5} sec ⁻¹)		1250
	133	0°	20 °C	D (10^2 sec ⁻¹)		1000
	T300/Epoxy 2500	0°	20 °C	S (10^{-5} sec ⁻¹)		750
		0°	20 °C	D (10^2 sec ⁻¹)		600
Chou et al. (1995)	T800H/3631	0°	20 °C	S	200	507
		45°	20 °C	S	450	580
		90°	20 °C	S	380	800
		0°	150 °C	S	200	
		45°	150 °C	S	500	
Asp (1998)	HTA/6376C	0°	20 °C	S	220	600
	carbon/epoxy Ciba	0°	100 °C	S	250	665
	Geigy	45°	20 °C	S		895
Ashcroft et al. (2001)	IM graphite fibers	0°	20 °C	S	500	
	bismaleimide/epoxy matrix		90 °C	S	1500	
Zitoun et al. (2007)	T700/M21 CFRP	0°	20 °C	S	330	1209
		45°	20 °C	S	440	1400

2.5. Energy release rate G_c

Delamination or interlaminar damage is one of the predominant failure modes in laminated composite systems since no reinforcement is present in the thickness direction. When drilling thin CFRP laminates, the usual propagation mode is mode I and the models previously described are based on this assumption. Similarly, for the interfaces of unidirectional layers of the same orientation, the elastic properties of these adjacent plies are the same, so that the propagation mode is unambiguous. However, when the plies bounding the delamination are of different orientations, loading modes become coupled due to the oscillatory nature of the stress and displacement near the crack front interface. The release rate of energy is also coupled and distributed into two or three failure modes.

In the case of CFRP laminates, although the n last plies can be assimilated to a thin plate, it is not so obvious that the propagation of the delamination is only in mode I. Delamination growth is likely to occur under mixed-mode loading since the composite material plate to drill is subjected to an axial force and bends. The mode II can then be activated. Furthermore, as reported by Park et al. (2013) or Montoya (2013) and as confirmed during the tests, the

temperature of the CFRP during drilling can increase up to 90 °C. The composite material is then stressed at a temperature well above ambient temperature but supposed to be constant in the last ten plies. The values of G_{IC} , G_{IIc} or G_c for respectively mode I, mode II or mixed mode failure have to reflect these conditions of loading and temperature.

During the drilling phase, although the tool impacts the plate in such a way the deflection shape and amplitude are equivalent to a static loading case, it is dynamically rotating and constantly fed forward, generating in the CFRP an intensive dynamical load which can not only intensify delamination generations but also directly cause them.

The energy release rate has to reflect these behaviors: incorporate a mixed-mode formulation with dynamic values of G_{IC} ($i = I, II$ or III) better than static ones, at a temperature different than room temperature.

The most widely used criterion to predict delamination propagation under mixed-mode loading is the power law criterion, established in terms of an interaction between the energy release rates:

$$\left(\frac{G_I}{G_{IC}}\right)^\mu + \left(\frac{G_{II}}{G_{IIc}}\right)^\mu + \left(\frac{G_{III}}{G_{IIIc}}\right)^\mu = 1 \quad (20)$$

Ladevèze et al. (1998) determined the values of α for carbon fiber/epoxy resin composites with different ply disorientation in quasi-static loading. The μ value is equal to 1.59, 1.12 and 1.19 for a disorientation of respectively 0° , 45° and 90° .

However, the mixed-mode criterion proposed by Benzeggagh and Kenane (1996) gives better results over a comprehensive range of mode mixity and allows linking the equivalent energy release rate G_C to G_{IC} and G_{IIC} through the following relation (B-K criterion):

$$G_C = G_{IC} + (G_{IIC} - G_{IC}) \beta^n \quad (21)$$

where the coefficient β has been defined by Hu et al. (2008) as $\beta = \delta_{\text{shear}}/\delta_{\text{axial}}$. This coefficient varies with the number n of plies to be drilled and with the cutting conditions.

However there is a lack of data in the literature for values of G_{IC} , G_{IIC} or G_{IIIC} for CFRP made of T800 carbon fibers and 923C epoxy resin, at ambient temperature or not, or depending on the orientation of the plies where delamination occurs. Data for similar CFRP have been compiled in Table 1.

These different data show disparities in the results. The critical energy release rate is highly dependent on the resin toughness, the disorientation between the plies, the temperature and the shear strain rate.

These studies point out that (i) the quality of the holes, and in particular delamination, directly affects the in-service behavior of CFRP; (ii) the delamination is directly associated with the geometry of the drill and its cutting edges, the cutting conditions and

particularly the feed rate which controls the axial force; (iii) an analytical model and a cutting empirical law associating the axial force to the cutting parameters (mainly feed rate and diameter of the drill) makes possible to control the drilling process in order to avoid delamination.

But they also demonstrate the lack of knowledge that currently exists concerning the modelling of cutting edge load distribution to be used for a given tool. An effort should be made in this way. It is also important to take into account the anisotropy of the material that remains to be drilled and to know more accurately the delamination propagation modes.

3. Experimental evaluation of the cutting edge loading

To determine analytically the critical thrust force, it is important to have an idea of the distribution of the cutting force on the tool cutting edge as a function of the drilling conditions, in particular the feed rate.

Tests have been performed using a Sandvik CoroDrill R846 twist drill which is suitable for titanium-based alloys and CFRP drilling. The material used in the experiments is a CFRP composite material made of intermediate modulus T800 carbon fibers and 924C epoxy resin. It consists of 100 plies having the same 0.182 mm thickness, where the eight final layers are oriented as follows: $45^\circ/45^\circ/90^\circ/90^\circ/45^\circ/45^\circ/0^\circ/45^\circ$.

Table 2

Experimental load (N) and intensity q (N/mm²) distributed over the referred intervals measured along the cutting edge from the center of the drill, for different feed rates and a cutting speed of 90 m/min.

f	Ø 0- Ø 3,9 mm		Ø 3,9- Ø 5,2 mm		Ø 5,2- Ø 6,6 mm		Ø 6,6- Ø 8 mm		Ø 8- Ø 9,4 mm		Ø 9,4- Ø 10,8 mm		Ø 0-Ø 10,8 mm
mm/rev	Fa	q	Fa	q	Fa	q	Fa	q	Fa	q	Fa	q	Fa
N	N	N/mm ²	N	N/mm ²	N	N/mm ²	N	N/mm ²	N	N/mm ²	N	N/mm ²	N
0.03	102	8.54	55	5.92	53	4.09	33	2.06	30	1.57	24	1.08	297
0.09	145	12.14	59	6.35	57	4.40	31	1.93	25	1.31	20	0.90	337
0.15	226	18.93	62	6.68	57	4.40	37	2.31	19	0.99	20	0.90	421
0.2	281	23.53	66	7.11	57	4.40	34	2.12	22	1.15	20	0.90	480
0.25	365	30.57	66	7.11	54	4.16	37	2.31	22	1.15	20	0.90	564

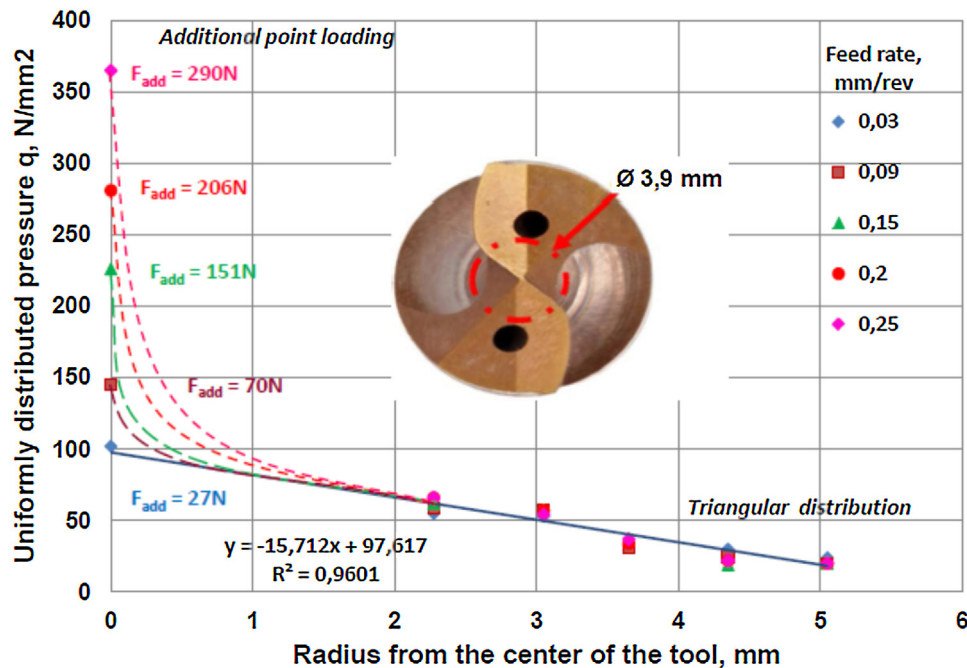


Fig. 5. Uniformly distributed pressure q of the load distributed over the referred intervals measured along the cutting edge from the center of the drill.

The drills have a diameter of 10.8 mm. Pilot holes of 3.9 mm, 5.2 mm, 6.6 mm, 8 mm and 9.4 mm in diameter have been drilled in order to discretize the cutting edge and be able to evaluate the corresponding loads for each interval. The tests have been done using a constant cutting speed of 90 m/min and a varying feed rate since this parameter is more influent on the axial load than the cutting speed. The feed rate values used are 0.03 mm/rev, 0.09 mm/rev, 0.15 mm/rev, 0.20 mm/rev and 0.25 mm/rev. The axial load F_a and the torque were recorded using an Artis system associated to a PC with Labview software. The results of the measured load and the uniformly distributed pressure q of the axial load referring to the corresponding surface area are given in Table 2. This repartition is clearly triangular (Fig. 5) with an additional loading for the center part of the drill.

This additional loading is highly dependent on the feed rate. The cutting edge is then loaded as follows:

- for a feed rate lower than 0.09 mm/rev, the loading is triangular along the cutting edge and the chisel edge.
- for a feed rate equal or higher than 0.09 mm/rev, the loading is triangular along the cutting edge and becomes non-linear converging towards an additional located loading on the chisel edge. This central part corresponds to the drill chisel edge after which there is a slope change of the cutting edge and a variation of the point angle (Fig. 5).

Table 3 gives the values of the additional point loading force and the corresponding value α of the repartition of load between triangular and point forces, with $F_{add} = (1 - \alpha) F_a$. The value of α varies linearly with the feed rate as follows: $\alpha = 0.975 - 1.840 f$ with a coefficient of regression of the fit function of 0.998.

4. New models

4.1. Point loading

In this case, it is assumed that the thrust force is exerted mainly by the chisel edge of the tool and therefore the loading will be concentrated in the center of the plate (Fig. 6a). Q is related to the axial force F_z distributed over the plate as follows:

$$Q2\pi r = F_z \Rightarrow Q = \frac{F_z}{2\pi r} \quad (22)$$

Substituting Q in the general formula (11), integrating and applying the boundary conditions of a clamped plate on its periphery, the deflection of the plate subjected to a concentrated or point load in its center can be obtained:

$$w(r) = \frac{F_z}{8\pi D} \left(r^2 \ln \frac{r}{a} + \frac{a^2 - r^2}{2} \right) \quad (23)$$

With the following expressions for the work done by the thrust force, the infinitesimal strain energy and the delamination energy:

$$\delta W_{ext} = \frac{1}{8} \frac{F_z^2 a}{\pi D} \delta a \quad \delta U = \frac{3}{64} \frac{F_z^2 a}{\pi D^2} D' \delta a \quad \delta U_d = 2G_C \pi a \delta a \quad (24)$$

the critical thrust will be finally:

$$F_z = 4\pi \sqrt{\frac{G_C D}{3D'}} \quad (25)$$

4.2. Triangular loading

As pointed out by the experiment, triangular loading seems to be the most convenient for the problem considered in this study. This model allows higher loading on the chisel edge than on the two main edges (Fig. 6b). Taking into account that the linearly

distributed load can be written as $q = Ar + B$, the general Eq. (11) can be rewritten as:

$$\frac{d}{dr} \left\{ r \frac{d}{dr} \left[\frac{1}{r} \frac{d}{dr} \left(r \frac{dw}{dr} \right) \right] \right\} = \frac{Ar^2 + Br}{D} \quad (26)$$

By integrating and applying the boundary conditions of a plate clamped on its periphery, the deflection of the plate is given by Eq. (27):

$$w(r) = \frac{1}{14400D} (r - a)^2 \left(96Aa^3 + 225Ba^2 + 192rAa^2 + 128Aar^2 + 450raB + 225Br^2 + 64Ar^3 \right) \quad (27)$$

Where the two parameters A and B are related by the following relation:

$$F_z = \int_0^a \pi r^2 (Ar + B) dr \Rightarrow B = \frac{3F_z - 2\pi Aa^3}{3\pi a^2} \quad (28)$$

The deflection of the plate is then only a function of the parameter A , which is the slope of the load distribution. Then, the energy balance is re-applied with the following expressions of work and energies:

$$\delta W_{ext} = \frac{\pi}{7200D} \left[\frac{304}{21} A^2 a^6 - \frac{550}{7\pi} A F_z a^3 + \frac{75}{\pi^2} F_z^2 \right] a \delta a \quad (29)$$

$$\delta U = \frac{3\pi}{4} \frac{D'}{D^2} \left[\frac{76}{75600} A^2 a^6 - \frac{11}{2016} \frac{F_z A a^3}{\pi} + \frac{1}{192} \frac{F_z^2}{\pi^2} \right] a \delta a \quad (30)$$

$$\delta U_d = 2G_C \pi a \delta a \quad (31)$$

The critical thrust force, in terms of A since depending on the tool used, is then:

$$F_z = Aa^3 \pi \left(\frac{11}{21} + \sqrt{\frac{299}{3675} + 64 \frac{D}{D'} \frac{G_C}{A^2 a^6}} \right) \quad (32)$$

Where:

$$D' = \left[\frac{1}{3} - \frac{D'}{8D} \right]; D = \frac{1}{3} (3D_{11} + 2D_{12} + 4D_{66} + 3D_{22})$$

$$\text{and } D' = \frac{D_{11} + D_{22}}{2} + \frac{D_{12} + D_{66}}{3} \quad (33)$$

For small diameters (diameter $2a$ up to 10 mm), the term Aa^3 is very small and the critical axial load can be expressed as follows:

$$F_z = \frac{11A\pi a^3}{21} + A\pi a^3 \sqrt{\frac{64G_{lc}}{A^2 a^6} \frac{D}{D'}} \sqrt{1 + \frac{299}{3675} \frac{D'}{D} \frac{A^2 a^6}{64G_{lc}}} \approx 8\pi \sqrt{G_{lc} \frac{D}{D'}} \quad (6)$$

This means that for small drill diameters, the triangular loading is similar to the uniformly distributed loading of the Piquet's model, Eq. (6).

4.3. Generalized composed loading

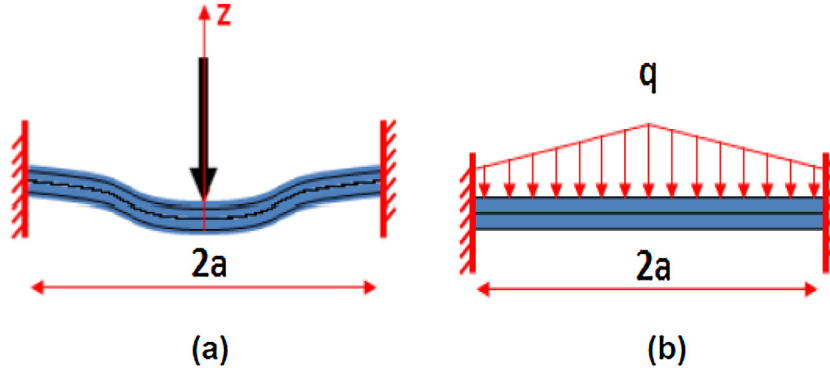
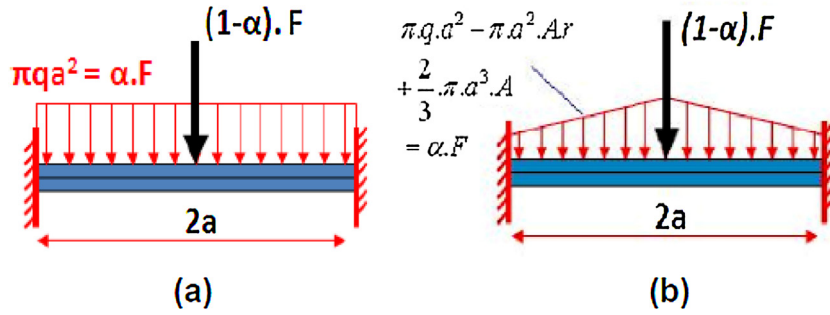
The modeling of such loads is more complex and is based on the principle of superimposition and the hypothesis of elastic behavior and small deflections.

4.3.1. Uniform loading with additional force located in the centre of the plate

Although the previous triangular loading takes into account the forces generated by the drill chisel edge and by the cutting edges, the following model considers that the force exerted by the chisel edge is higher. Part of the applied force is modeled as a point force at the center of the plate, on the chisel edge, and the other part as a uniform load along the two main edges as well as the chisel edge (Fig. 7a).

Table 3Values of F_{add} and α for the different feed rates used.

f (mm/rev)	0.03	0.09	0.15	0.20	0.25
F_{add} (N)	27	70	151	206	290
α	0.92	0.82	0.68	0.61	0.52

**Fig. 6.** Deflection of a clamped plate subjected to (a) a punctual load in its center and (b) a triangular loading.**Fig. 7.** Combined loading consisting in (a) point loading on the drill web and uniform distributed loading on the two main cutting edges and the web and (b) point loading on the drill web and triangular loading on the two main cutting edges and the web.

The deformation energy and the work of external forces can be calculated from both simple cases, the point load subjected to a force $(1-\alpha).F$ and uniformly distributed load equivalent to $\alpha.F$ and the final value corresponding to the combined loading is the sum of the values obtained for each case. The energy balance is then given by Eq. (34):

$$(\delta W_{ext})_{point} + (\delta W_{ext})_{uniform} = (\delta U)_{point} + (\delta U)_{uniform} + \delta U_d \quad (34)$$

The expression for the critical stress is then:

$$F_z = 8\pi \sqrt{\frac{G_c}{\alpha^2 + 12(1-\alpha)^2} \frac{D}{D''}} \quad (35)$$

For $\alpha=1/2$, and supposing that $D'/D \approx 4/3$, the result of Rahmé (Eq. 10) can be recovered:

$$F_z = 16\pi \sqrt{\frac{1}{13} \left(\frac{1}{3} \right) - \left(\frac{D'}{8D} \right)} \approx 16\pi \sqrt{\frac{6G_c D}{13}} \quad (10)$$

For $\alpha=0$ and $\alpha=1$, we obtain the relations (25) and (6), respectively associated to point loading and uniform loading.

4.3.2. Triangular loading with additional force located in the centre of the plate

Part of the applied force is modeled as a point force at the center of the plate, on the chisel edge, and the other as a triangular loading, along the two main edges and the chisel edge (Fig. 7b).

The deformation energy and the work of external forces can be calculated from the two simple cases, the point load subjected to a

force $(1-\alpha).F$ and the triangular load equivalent to $\alpha.F$. The final value corresponding to the combined loading is the sum of the values obtained for each case. The energy balance is then given by:

$$(\delta W_{ext})_{punctual} + (\delta W_{ext})_{triangular} = (\delta U)_{punctual} + (\delta U)_{triangular} + \delta U_d \quad (36)$$

The energy balance leads to the following second degree Eq. (37) for calculating the critical force:

$$\left[12(1-\alpha)^2 + \alpha^2 \right] \cdot F_z^2 - \frac{22}{21} \cdot \pi \cdot \alpha \cdot A \cdot a^3 \cdot F_z + \frac{304}{1575} \cdot \pi^2 \cdot A^2 \cdot a^6 - 64 \cdot \pi^2 \cdot G_c \frac{D}{D''} = 0 \quad (37)$$

and the critical force is then:

$$F_z = \frac{\frac{22}{21} \pi \alpha A a^3 \pm \sqrt{\Delta}}{2 \left[12(1-\alpha)^2 + \alpha^2 \right]} \quad (38)$$

With

$$\Delta = \pi^2 A^2 a^6 \left[\frac{10764 \cdot \alpha^2 - 306432 \cdot (1-\alpha)^2}{33075} \right] + 256 \cdot \pi^2 G_c \frac{D}{D''} \left[12(1-\alpha)^2 + \alpha^2 \right] \quad (39)$$

For $\alpha=0$ and $\alpha=1$, Eqs. (25) and (32), respectively associated to point loading and triangular loading can be recovered.

4.4. Experimental determination of critical loads for the delamination of n plies

A second trial of experiments has been done in order to determine correlations between the thrust force generated by drills of

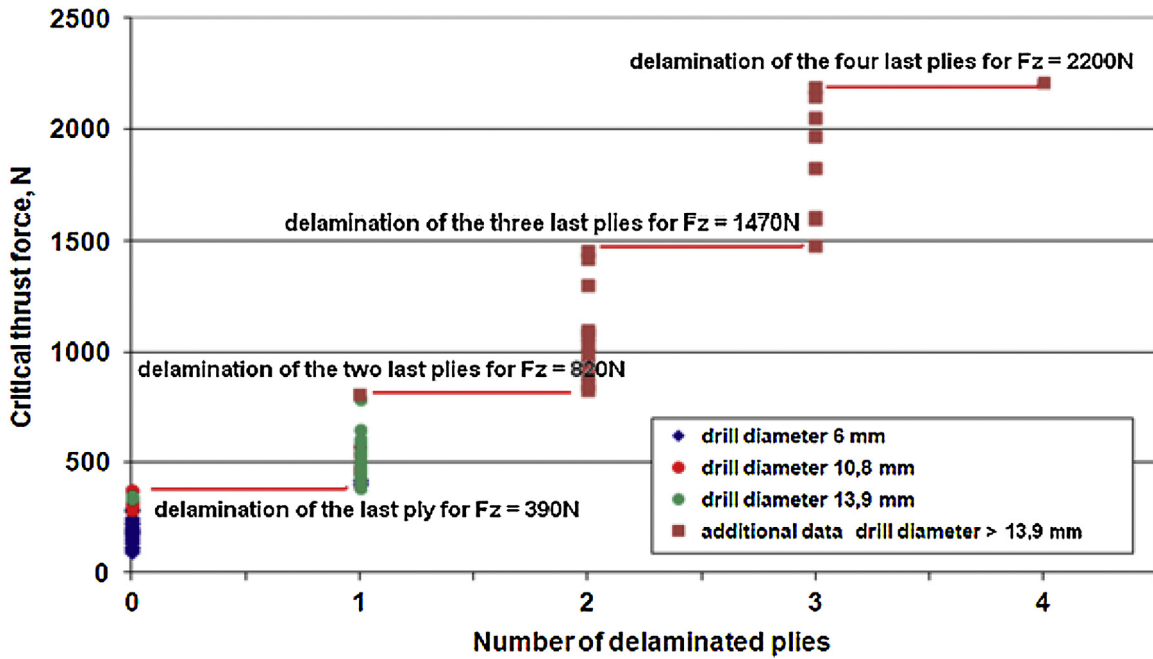


Fig. 8. Evolution of the critical thrust force with the number of delaminated plies.

different diameter on one hand and the occurrence of one or various delaminated layers in the composite on the other hand.

The tests have been carried out on the same CFRP material using the same Sandvik CoroDrill R846 tool geometry with diameters of 6 mm, 10.8 mm, 13.9 mm and higher. The same procedure has been used for measuring thrust force and torque for each experiment.

The Design of Experiment carried out consists in an orthogonal design with three different cutting speeds (45, 90 and 135 m/min) and three different feed rates (0.03; 0.09 and 0.15 mm/rev) for each different diameter. Each experiment is done twice in order to take into account tool wear. The specimens are cut in order to determine the number of delaminated plies (Fig. 4b).

The results are summarized in Fig. 8. It points out that to delaminate the last ply of the CFRP, it is necessary to reach experimentally a thrust force near 390 N whatever the tool diameter or the drilling conditions. For delamination of the two, three and four last plies, this critical thrust force is respectively 820 N, 1470 N and 2200 N. These values are of the same order than the results obtained by Zitoun et al. (2007, 2013) for T700GC/M21 composite laminates.

4.5. Determination of the energy release rate G_c

In order to compare these experimental results with the different models previously described, the following data for the T800/923C CFRP material have been used to calculate the critical thrust force for each case: $E_{11} = 150.31$ GPa; $E_{22} = 7.58$ GPa; $G_{12} = 3.93$ GPa; $\nu_{12} = 0.35$; Ply thickness = 0.182 mm (data from Aerospace Process Specifications).

Due to the lack of data concerning our materials, the determination of the unknown parameters, energy release rate G_{IC} and G_{IIC} , of the β and η coefficients, necessary to estimate the mixed mode energy release rate G_c of Eq. (21) is then done by an inverse method.

Taking into account that the critical thrust load for delamination must be identical for the five identified α values of load repartition, these parameters are determined minimizing the error between experimental values and the model, by multilinear regression, for each relation for the triangular + point loading of the cutting edge, for the different values of α . It has been found that the optimized values of G_{IC} , G_{IIC} , are respectively 500 J/m² and 3000 J/m² for a

disorientation of 0°, 600 J/m² and 4500 J/m² for a disorientation of 45° and 2.63 for η . The associated values of β are given in Table 4.

Table 4 points out that the mixed-mode is effective whatever the cutting conditions, the mode II being more active when the last ply is only loaded and when the cutting conditions are stronger (lower value of the α coefficient). In this last case, when only the last ply is loaded, the shear and axial deformations are similar. On the contrary, for higher values of α , which means lower cutting conditions and corresponding lower thrust loads, mode I is predominant (Fig. 4b) leading to low β values. The coefficient β is significantly correlated with the feed rate, the number of remaining plies and the coefficient α which is characteristic of the load distribution on the cutting edge as pointed out by an analysis of variance. The fit function is: $\beta = 3.252f - 0.104N_{ply} + 0.4791\alpha$, with a regression coefficient of the fit model of 0.997.

4.6. Comparison of new models and literature models with experimental data

Fig. 9 shows a comparison of the different models proposed in the literature: the triangular model, the triangular with additional force model and the experimental data. The models of the literature are not in total agreement with the experimental data whatever the values of G_{IC} in function of the disorientation angle. This means that using only mode I is not possible to explain the values of critical thrust force which have been measured. The triangular loading model (and also the uniform loading model) which has been developed leads to values which fit the experimental data better but this model is still too distant from these data. The models of Rahmé and Lachaud need higher values of critical energy release rate to fit the data (2150 and 3900 J/m² for Rahmé's model, 1700 and 3100 J/m² for Lachaud's model, respectively for 0 and 45° of disorientation). However, when using these values, the critical thrust load obtained for delamination of the three and four last plies is then 100% too high.

In the case of an elliptic delamination area assumption (Jain and Yang's model; Zhang's model), the values of the critical axial load are also too low compared with the experimental ones although the ellipticity ratio has been underestimated ($\xi = (D_{11}/D_{22})^{1/4} = 1.41$

Table 4

Values of $\beta = \delta_{\text{shear}} / \delta_{\text{axial}}$ for the different disorientations between plies, as a function of the delaminated ply number and the coefficient α .

Number of delaminated plies	1	2	3	4	1	2	3	4	1	2	3	4
Disorientation	45	0	45	45	45	0	45	45	45	0	45	45
Coefficient α	0.92				0.82				0.68			
β	0.518	0.357	0.165	0.158	0.568	0.426	0.273	0.268	0.737	0.623	0.478	0.475
Number of delaminated plies	1	2	3	4	1	2	3	4				
Disorientation	45	0	45	45	45	0	45	45				
Coefficient α	0.61				0.52							
β	0.838	0.728	0.575	0.572	0.97	0.862	0.692	0.689				

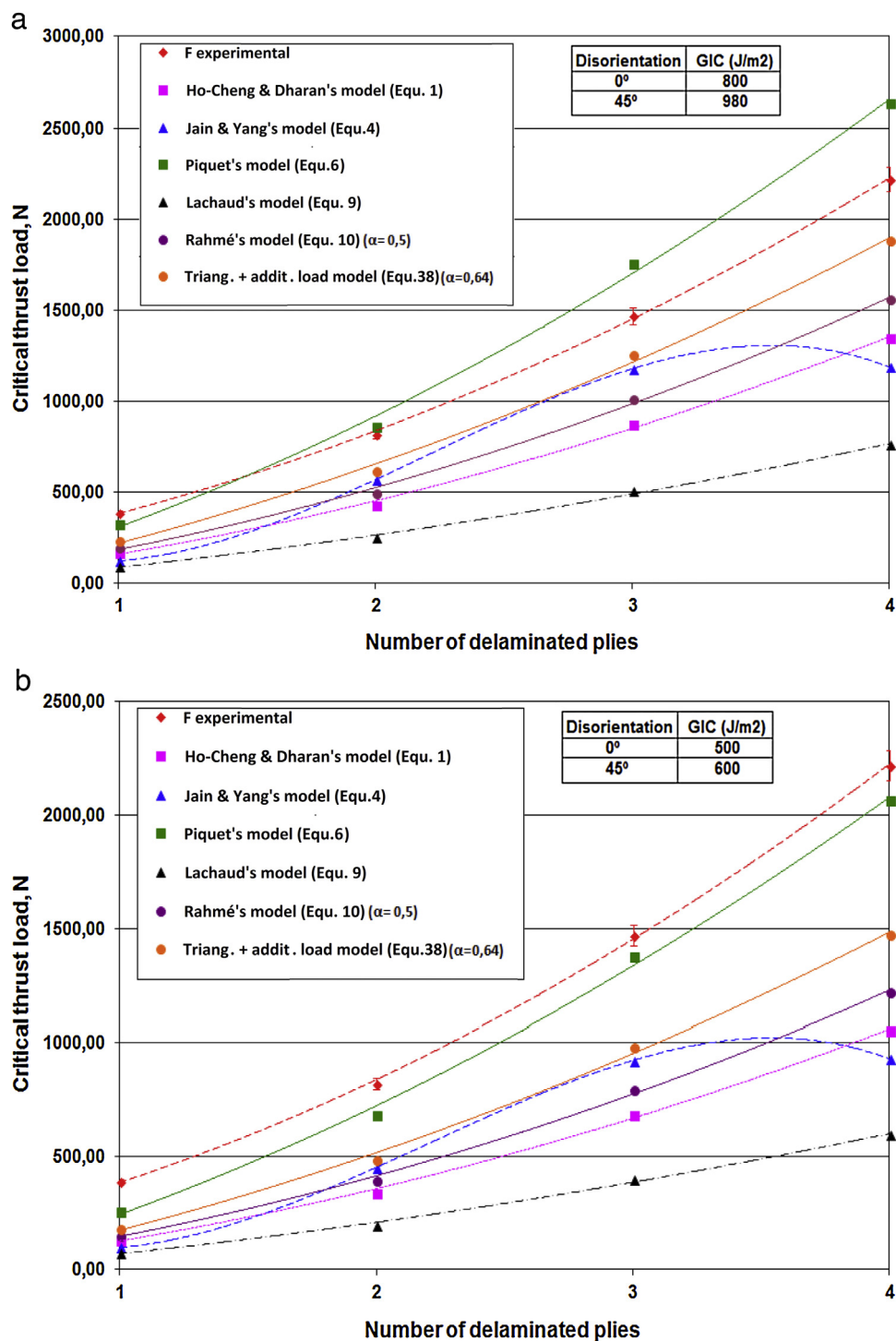


Fig. 9. Comparison between the different models of the literature, the new model and the experimental data.

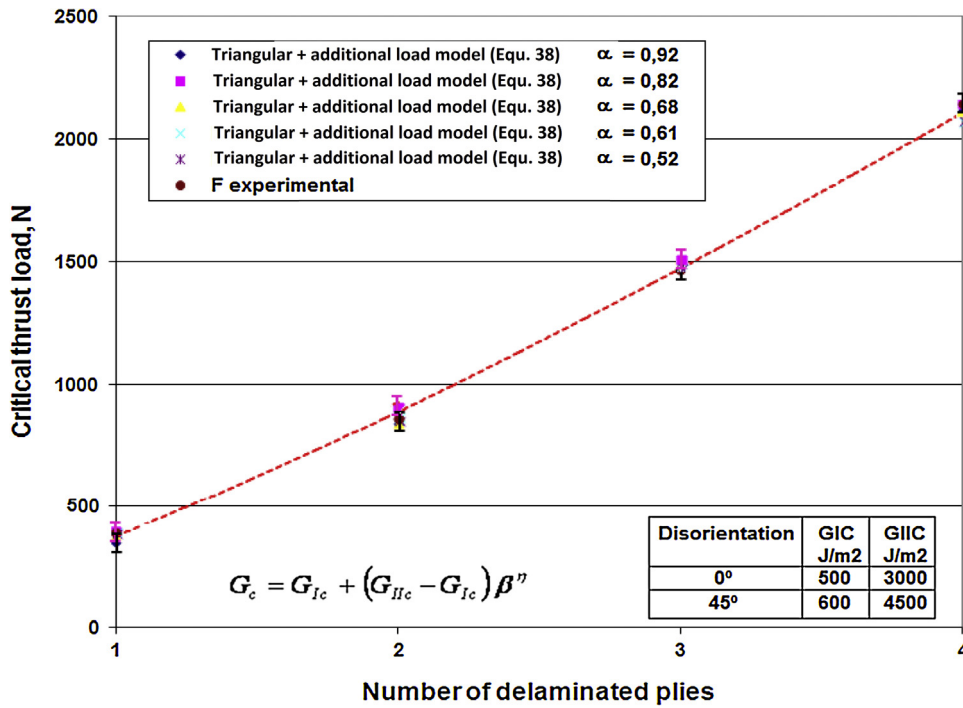


Fig. 10. Comparison between the new model for the different α values, and the experimental data (drill diameter 10,8 mm).

from Jain's relation and 1.63 from experiments). In that case also the model needs higher values of critical energy release (9600 and 1660 J/m² respectively for 0 and 45° of disorientation). However, when using these values, the critical thrust load obtained for delamination of the three and four last plies is then 150% too high.

These observations lead to the conclusion that mode I alone cannot explain the delamination behavior of the composite plate. They are confirmed by Zitoun and Collombet (2007) who have pointed out this fact in a numerical simulation, using the power law criterion (Eq. (20)) and a repartition of the axial load F_z between the cutting lips ($\alpha \cdot F_z$) and the chisel edge ($(1-\alpha) \cdot F_z$). Their numerical results have shown that the best fitting was obtained when the mixed-mode I/II and a value of the coefficient of distribution of the load α of 0.6 were used.

In the case of the triangular+point model developed here and associated with the B-K criterion and the values of β determined by linear regression (Table 4), the models are in good agreement with the experimental data whatever the values used for α (Fig. 10).

As we can see in Fig. 5, $\alpha \cdot F_a$ represents the triangular distribution of the load along the cutting edge. Due to the particular design of the drill, this contribution is constant whatever the cutting conditions. An increase of the feed rate leads to an increase of the additional load on the center of the drill and the load on the drill corners remain the same. This geometry should prevent delamination since the value of the effort at these points is low. If there is delamination, it may be due to the additional effort and the solicitation in mode I and II of the last plies. Then, this new analytical approach is able to take into account the coupling between bending and stretching commonly observed in CFRPs with various lay-ups, and to modulate these two effects according to the number of layers remaining to drill and their characteristics of stiffness and orientation. The effect of the load distribution on the web and chisel edges is also incorporated into this model and helps to improve the accuracy of the predictions.

5. Conclusions

This study has focused on three important aspects, (i) the distribution of the load along the drill edges, (ii) the development of a combined loading model with mixed mode delamination propagation and (iii) the experimental validation of this new model.

In the case of a Sandvik R846 twist drill, it has been demonstrated a triangular distribution of the pressure along the cutting and chisel edges associated to an additional load located at the center of the drill. This additional load depends strongly on the feed rate and follows a linear function.

This additional force represents 8% of the axial thrust for low feed rates and increases to 48% for high feed rates.

An orthotropic analytical model has been developed in order to determine the delamination critical thrust during drilling for different combined loadings. This new model takes into account the distribution of the pressure along the cutting and chisel edges previously determined and is based on a mixed mode I/II evolution of the delamination.

This new model has been compared with existing ones in the literature and with experimental results. Whatever the model used, the results do not agree very well with experiments when taking into account only mode I delamination.

The use of the B-K criterion to determine the equivalent critical energy release rate G_c and the cutting edge combined load distribution (triangular distribution associated to an additional load) allows a close correlation between experimental measurements and the prediction of this new model.

Acknowledgments

Part of this work has been supported by the Unit for Training and Research in Mechanical Engineering of the University of the Basque Country (UFI11/29). The authors also wish to thank Ugaitz

Orrantia, Begoña de Zarate-Knörr and Paula Arbe for their help in carrying out the experimental tests.

References

- Aerospace Process Specifications, Drilling of composites and composite/metallic assemblies, Airbus AIP1 01-02-005 and AIP1 01-02-003, Bombardier BAPS 188-007, Embraer: NE 40-273.
- Ashcroft, I.A., Hughes, D.J., Shaw, S.J., 2001. Mode I fracture of epoxy bonded composite joints: 1. Quasi-static loading. *Int. J. Adhes. Adhes.* 21, 87–99, [http://dx.doi.org/10.1016/S0143-7496\(00\)00038-5](http://dx.doi.org/10.1016/S0143-7496(00)00038-5).
- Asp, L.E., 1998. The effects of moisture and temperature on the interlaminar delamination toughness of a carbon/epoxy composite. *Compos. Sci. Technol.* 58, 967–977, [http://dx.doi.org/10.1016/S0266-3538\(97\)00222-4](http://dx.doi.org/10.1016/S0266-3538(97)00222-4).
- Benzeggagh, M.L., Kenane, M., 1996. Measurement of mixed-mode delamination fracture toughness of unidirectional glass/epoxy composites with mixed-mode bending apparatus. *Compos. Sci. Technol.* 56, 439–449, [http://dx.doi.org/10.1016/0266-3538\(96\)00005-X](http://dx.doi.org/10.1016/0266-3538(96)00005-X).
- Brinksmeier, E., Fangmann, S., Rentsch, R., 2011. Drilling of composites and resulting surface integrity. *CIRP Ann. – Manuf. Technol.* 60, 57–60, <http://dx.doi.org/10.1016/j.cirp.2011.03.077>.
- Chou, I., Kimpara, I., Kageyama, K., Ohsawa, I., 1995. Mode I and mode II fracture toughness measured between differently oriented plies in graphite/epoxy composites. *ASTM, STP-1230*, 132–151, <http://dx.doi.org/10.1520/STP14012S>.
- De Zarate Knörr, B., 2014. *Optimisation Du Processus De Perçage d'empilages Hybrides Composites/Titane*, Master Thesis. ENSAM, Bordeaux, France, BO –M14008.
- Ho-Cheng, H., Dharan, G.K.H., 1990. Delamination during drilling in composite laminates. *Trans. ASME* 112, 236–239, <http://dx.doi.org/10.1115/1.2899580>.
- Hocheng, H., Tsao, C.C., 2003. Comprehensive analysis of delamination in drilling of composite materials with various drill bits. *J. Mat. Proc. Technol.* 140, 335–339, [http://dx.doi.org/10.1016/S0924-0136\(03\)00749-0](http://dx.doi.org/10.1016/S0924-0136(03)00749-0).
- Hocheng, H., Tsao, C.C., 2005. The path towards delamination-free drilling of composite materials. *J. Mat. Proc. Technol.* 167, 251–264, <http://dx.doi.org/10.1016/j.jmatprotec.2005.06.039>.
- Hocheng, H., Tsao, C.C., 2006. Effects of special drill bits on drilling-induced delamination of composite materials. *Int. J. Mach. Tools Manuf.* 46, 1403–1416, <http://dx.doi.org/10.1016/j.ijmachtools.2005.10.004>.
- Hu, N., Zemba, Y., Okabe, T., Yan, C., Fukunaga, H., Elmarakbi, A.M., 2008. A new cohesive model for simulating delamination propagation in composite laminates under transverse loads. *Mech. Mater.* 40, 920–935, <http://dx.doi.org/10.1016/j.mechmat.2008.05.003>.
- Iliescu, D., Gehin, D., Iordanoff, I., Girot, F., Gutiérrez, M.E., 2010. A discrete element method for the simulation of CFRP cutting. *Compos. Sci. Technol.* 70, 73–80, <http://dx.doi.org/10.1016/j.compscitech.2009.09.007>.
- Jain, S., Yang, D.C.H., 1993. Effects of feed rate and chisel edge on delamination in composites drilling. *Trans. ASME* 115, 398–405, <http://dx.doi.org/10.1115/1.2901782>.
- Jain, S., Yang, D.C.H., 1994. Delamination-free drilling of composite laminates. *J. Eng. Ind.* 116, 475–481, <http://dx.doi.org/10.1115/1.2902131>.
- Jawahir, I.S., Brinksmeier, E., M'saoubi, R., Aspinwall, D.K., Outeiro, J.C., Meyer, D., Umbrello, D., Jayal, A.D., 2011. Surface integrity in material removal processes: recent advances. *CIRP Ann. – Manuf. Technol.* 60, 603–626, <http://dx.doi.org/10.1016/j.cirp.2011.05.002>.
- Kusaka, T., Kurokawa, T., Yamauchi, Y., 1994. Estimation of dynamic interlaminar fracture toughness of CFRP by ENF test using SHPB method. II. strain rate dependence of mode II interlaminar fracture toughness of unidirectional CF/Epoxy composite laminates. *J. Soc. Mater. Sci. Jpn.* 43 (487), 445.
- Lachaud, F., Piquet, R., Collombet, F., Surcin, L., 2001. Drilling of composites structures. *Comp. Struct.* 52, 511–516, [http://dx.doi.org/10.1016/S0263-8223\(01\)00040-X](http://dx.doi.org/10.1016/S0263-8223(01)00040-X).
- Ladevèze, P., Allix, O., Douchin, B., Lévêque, D., 1998. A computational method for damage intensity prediction in a laminated composite structure. In: Idelsohn, S., Oñate, E., Dvorkin, E. (Eds.), *Computational Mechanics, New Trends and Applications*. CIMNE, Barcelona, Spain, pp. 1–14.
- Montoya, M., 2013. *Optimisation Du Perçage d'empilages CFRP/Titane Et/ou Aluminium*, PhD Thesis No 2013-ENAM-00xx, École Doctorale No432: Sciences Des Métiers De l'Ingénieur. Arts et Métiers ParisTech.
- Park, J.-M., Kwon, D.J., Wang, Z.-J., Gu, G.-Y., DeVries, K.L., 2013. A new strategy of carbon fiber reinforced plastic drilling evaluation using thermal measurement. *J. Compos. Mater.* 47 (16), 2005–2011, <http://dx.doi.org/10.1177/0021998312453358>.
- Persson, E., Eriksson, I., Zackrisson, L., 1997. Effects of hole machining defects on strength and fatigue life of composite laminates. *Compos. Part A* 28A, 141–151, [http://dx.doi.org/10.1016/S1359-835X\(96\)00106-6](http://dx.doi.org/10.1016/S1359-835X(96)00106-6).
- Piquet, R., Ferret, B., Lachaud, F., Swider, P., 2000. Experimental analysis of drilling damage in thin carbon/epoxy plate using special drills. *Compos. Part A* 31, 1107–1115, [http://dx.doi.org/10.1016/S1359-835X\(00\)00069-5](http://dx.doi.org/10.1016/S1359-835X(00)00069-5).
- Rahmé, P., Landon, Y., Lachaud, F., Piquet, R., Lagarrigue, P., 2011. Analytical models of composite material drilling. *Int. J. Adv. Manuf. Technol.* 52, 609–617, <http://dx.doi.org/10.1007/s00170-010-2773-5>.
- Saleem, M., Toubal, L., Zitoun, R., Bougherara, H., 2013. Investigating the effect of machining processes on the mechanical behavior of composite plates with circular holes. *Compos. Part A: Appl. Sci. Manuf.* 55, 169–177, <http://dx.doi.org/10.1016/j.compositesa.2013.09.002>.
- Timoshenko, S., Woinowski-Krieger, S., 1987. *Theory of plates and shells, Chapter 3. In: Symmetrical Bending of Circular Plates*, Second edition. McGraw-Hill Book Company, pp. 51–78.
- Tsao, C.C., Chen, W.C., 1997. Prediction of the location of delamination in the drilling of composite laminates. *J. Mat. Proc. Technol.* 70, 185–189, [http://dx.doi.org/10.1016/S0924-0136\(97\)00059-9](http://dx.doi.org/10.1016/S0924-0136(97)00059-9).
- Tsao, C.C., Hocheng, H., 2003. The effect of chisel length and associated pilot hole on delamination when drilling composite materials. *Int. J. Mach. Tools Manuf.* 43, 1087–1092, [http://dx.doi.org/10.1016/S0890-6955\(03\)00127-5](http://dx.doi.org/10.1016/S0890-6955(03)00127-5).
- Tsao, C.C., Hocheng, H., 2004. Taguchi analysis of delamination associated with various drill bits in drilling of composite material. *Int. J. Mach. Tools Manuf.* 44, 1085–1090, <http://dx.doi.org/10.1016/j.ijmachtools.2004.02.019>.
- Tsao, C.C., Hocheng, H., 2007. Effect of tool wear on delamination in drilling composite materials. *Int. J. Mech. Sci.* 49, 983–988, <http://dx.doi.org/10.1016/j.jimecsci.2007.01.001>.
- Tsao, C.C., Hocheng, H., 2008. Evaluation of thrust force and surface roughness in drilling composite material using Taguchi analysis and neural network. *J. Mat. Proc. Technol.* 203, 342–348, <http://dx.doi.org/10.1016/j.jmatprotec.2006.04.126>.
- Tsao, C.C., Hocheng, H., Chen, Y.C., 2012. Delamination reduction in drilling composite materials by active backup force. *CIRP Ann. – Manuf. Technol.* 61, 91–94, <http://dx.doi.org/10.1016/j.cirp.2012.03.036>.
- Zhang, L.-B., Wang, L.-J., Liu, X.-Y., 2001. A mechanical model for predicting critical thrust forces in drilling composite laminates. *Proceedings of the Institution of Mechanical Engineers, Part B: Journal of Engineering Manufacture* 215, 135–146, <http://dx.doi.org/10.1243/0954405011515235>.
- Zitoun, R., 2013. *Délamination lors du perçage d'un composite carbone-époxy*, Techniques de l'ingénieur, RE227, 1–10.
- Zitoun, R., Collombet, F., 2007. Numerical prediction of the thrust force responsible of delamination during the drilling of the long-fibre composite structures. *Composites: Part A* 38, 858–866, <http://dx.doi.org/10.1016/j.compositesa.2006.07.009>.